Published in "Trends in Parasitology 35(3): 193–212, 2019"
which should be cited to refer to this work.

Toolbox for *In Vivo* Imaging of Host–Parasite Interactions at Multiple Scales

Mariana De Niz,[1,2,7,8,*] Florentin Spadin,[3,8] Matthias Marti,[2] Jens V. Stein,[4,5] Martin Frenz,[3] and Friedrich Frischknecht[6]

Animal models have for long been pivotal for parasitology research. Over the last few years, techniques such as intravital, optoacoustic and magnetic resonance imaging, optical projection tomography, and selective plane illumination microscopy developed promising potential for gaining insights into host–pathogen interactions by allowing different visualization forms *in vivo* and *ex vivo*. Advances including increased resolution, penetration depth, and acquisition speed, together with more complex image analysis methods, facilitate tackling biological problems previously impossible to study and/or quantify. Here we discuss advances and challenges in the *in vivo* imaging toolbox, which hold promising potential for the field of parasitology.

Highlights

Technological advances in IVM include ultrafast tunable infrared lasers, super-resolution imaging *in vivo*, and better access to all organs by improved optics or motion-correction mechanisms.

Optical clearance methods for use in OPT and SPIM allow imaging entire organs and organisms (such as mice or insect vectors), while achieving cellular and subcellular resolution.

OAI combines optics and acoustics via the thermoelastic effect to investigate molecular mechanisms.

Key advances in MRI include improved contrast agents, multimodal mesoscopic imaging, and functional MRI to visualize the metabolic function of tissues.

Developments in bioluminescence imaging include red-shifted probes with high sensitivity; a larger diversity of probes with emission peaks at various wavelengths; ultrabright probes, and the use of BRET *in vivo*.

X-ray-based and gamma-ray-based imaging platforms are noninvasive and enable the study of anatomical structures, metabolism, biochemical composition of tissues, and dynamics.

Imaging Toolbox in Parasitology

Imaging techniques developed for biomedical applications have had an important impact in parasitology research. Such techniques include platforms developed to image host–pathogen interactions at various scales, ranging from molecules to whole organisms (summarized in Table 1). These techniques have complementary advantages with respect to each other. This review focuses on the technological advances used for visualization of host–pathogen interactions either *in vivo,* or *ex vivo* in whole organisms in several imaging techniques. These techniques are based on nonionizing radiation such as intravital microscopy (IVM), optical projection tomography (OPT), bioluminescence imaging, optoacoustic imaging (OAI), and magnetic resonance imaging (MRI), or on ionizing radiation such as X-ray micro-computed tomography (micro-CT), positron emission tomography (PET), or single-photon emission computed tomography (SPECT).

Advanced Fluorescence Methods Applied to IVM

IVM is a powerful technique for investigating dynamic cellular processes and host–parasite interactions within functioning organs. Organs studied by IVM in the context of parasitology include the brain [1–4], the skin [5–12], the lungs [13], the liver [14–18], the spleen [19,20], the intestines [21,22], the lymph nodes [23,24], the bone marrow [25], the adipose tissue [20], and the placenta [26,27], (summarized in Table 2). Important advances in parasitology have been achieved using wide-field epifluorescence, confocal, spinning-disc, or two-photon IVM. Recent developments, which have expanded the applications of IVM include the generation of longer wavelength excitation lasers; a wider range of fluorescent reporters for dyes; transgenic fluorescence reporter mice and parasites; **fluorescence lifetime** measurements (see Glossary); **adaptive optics**; **imaging windows** and microendoscopes, but also software advances for high-throughput automated analyses and motion correction. Moreover, for fixed specimens, tissue-clearing techniques providing deeper optical penetration into organs have opened new avenues of research [28].

[1]Institute of Cell Biology – Heussler Laboratory, University of Bern, Bern, Switzerland
[2]Wellcome Centre for Molecular Parasitology, University of Glasgow, Glasgow, Scotland, UK
[3]Institute of Applied Physics, University of Bern, Bern, Switzerland
[4]Theodor Kocher Institute, University

Longer wavelength excitation lasers offer substantial advantages for IVM. Wavelengths in the 700–1000 nm excitation range are to some extent limited by penetration depth and background emission from tissue endogenous signals. Ultrafast tuneable infrared lasers are now available which enable imaging at 1300 nm, overcoming both problems [29]. Longer wavelength light is less scattered and absorbed by tissues, as long as the wavelength is shorter than the water absorption peaks, resulting in deeper optical penetration. This new generation of lasers, coupled with novel far-red probes, take advantage of wavelengths that elicit fewer autofluorescence signals, thus helping to improve the signal-to-noise ratio. Moreover, phototoxicity to tissues is believed to be reduced at longer wavelengths [30]. Further, wavelength mixing of synchronized lasers, or multiphoton excitation – achieved either via dual-output laser sources or specialized lasers such as the recently reported femtosecond diamond Raman laser [31] – enable multicolour imaging, expanding the range of structures that can be studied *in vivo* by IVM. In parallel, a wide range of fluorescent probes in the form of immunofluorophores, genetic tags, quantum dots, and organic dyes have been developed to study dynamic processes *in vivo*, including protein–protein interactions, and host–pathogen interactions in healthy and diseased states (reviewed in [32,33]).

Microscopy tools that are key to investigating cell or protein dynamics, and interactions *in vitro*, have in recent years successfully permeated into IVM (reviewed in [34]). Examples of these methods include **Förster resonance energy transfer (FRET)**, **fluorescence loss in photobleaching (FLIP)**, and **fluorescence recovery after photobleaching (FRAP)**. FRET in mice has been achieved by either of two methods: generation of transgenic animals with chromophores acting as partners for resonance energy transfer, or transfection of cells followed by their transfer into living animals [35]. FRET poses important challenges in IVM, which are usually not encountered in *in vitro* conditions. These include signal strength limitations, **photobleaching** and photodamage. Initially, FRET was mostly used as a ratiometric technique in IVM, allowing the measurement of relative changes of different parameters of interest at high speed, generally using the fluorescent proteins cerulean and citrine as donor and acceptor fluorophores, respectively. Despite the value of ratiometric FRET, one of its main limitations is its dependence on relative quantifications rather than absolute measurements. So far, FRET has not been reported *in vivo* in parasitology, yet could be very useful to monitor the activity of kinases, proteases, and GTPases [36]; calcium changes [37]; lipid concentrations [35,38–40] during infection; and even physical stresses such as temperature, mechanical stressors, or electromagnetic fields [41], as well as molecular interactions between host and pathogens; host cell subsets, or parasite molecules. Likewise, there has been significant progress in the development of software to allow separate quantification of signals from single cells in complex 3D environments, such as those present in organs of living animals [42,43].

Another set of fluorescence methods increasingly adapted to IVM are FRAP and FLIP. Both techniques are generally used to monitor the molecular movement within cells, and are amenable to repeated use *in vivo* without causing tissue damage. They are particularly useful to assess macromolecular flux across cells and tissues. Both methods yield information such as half-time to recovery, rate of movement of fluorescent molecules within and between cellular compartments, and molecular transfer between regions independent of rate of movement. Like FRET, FRAP and FLIP have been largely explored in 2D environments using cell cultures, but have only recently been incorporated into *in vivo* research [34]. This has been possible due to the generation of transgenic mice with fluorescent reporters expressed in specific cell types, cell–cell junctions, or other structures. Particularly useful for the study of parasite cell migration, invasion, and development, would be reporter mice that enable quantification of dynamic

of Bern, Bern, Switzerland
[5]Department of Oncology, Microbiology and Immunology, University of Fribourg, Fribourg, Switzerland
[6]Integrative Parasitology, Centre for Infectious Diseases, Heidelberg University Medical School, Heidelberg, Germany
[7]Current affiliation: Instituto de Medicina Molecular – João Lobo Antunes, Faculdade de Medicina, Universidade de Lisboa, Lisbon, Portugal
[8]These authors contributed equally

*Correspondence:
mariana.deniz@medicina.ulisboa.pt
(M. De Niz).

regulation of cell–cell junctions (e.g., E-cadherin–GFP) [44], or studying microvessel leakiness as a proxy of endothelial barrier function using dyes such as fluorescein isothiocyanate-dextran or albumin [45].

Super-resolution microscopy has gained significant momentum for use in *in vitro* imaging over the past decade, and its application in IVM contexts brings about equally exciting prospects. One limitation that prevented its faster adaptation to IVM is the light scattering which results in depth-dependent deterioration of spatial resolution, due to spherical aberrations to the point spread function in complex tissue [46]. Although not yet used in the field of parasitology, other fields have developed methods to achieve super-resolution microscopy while imaging living animals. Examples include a recently developed setup which incorporates multibeam striped illumination, spatial modulation of excitation, and laser scanning microscopy [47], or the use of **stimulated emission depletion (STED)** to achieve super-resolution to observe morphological changes in actin within the brain [48].

In addition to microscopy methods applicable to IVM, the use of implanted optical windows to replace the skull, and microendoscopes, has greatly benefited various research fields, including parasitology, to enable long-term imaging of organs throughout multiple days (reviewed in [49]). While most optical windows are limited to the surface of the surgically exposed organs, **gradient index (GRIN) lenses** and microendoscopes enable access to deeper regions [50], otherwise inaccessible, including deeper structures in the brain, the spinal cord, the bone marrow, the lungs, and the heart [50–53]. Both microendoscopes and temporary optical windows have benefited the imaging of parasites, giving insights into phenomena including parasite crossing of endothelial barriers enabling their dissemination across tissues, dynamics relevant to parasite survival, and mechanisms of transmission to and from the insect vectors. Further progress in penetration depth and resolution in living samples has been achieved by adaptive optics, which is widely applied in astronomy. Biological specimens have refractive-index inhomogeneities which affect resolution. Adaptive optics allows reversing signal/resolution degradation by predistorting the wavefront of the incoming light to cancel distortions occurring in the light path [54].

Finally, a significant challenge for IVM is motion induced by breathing, peristalsis, and circulation, which mostly affects organs in the chest and abdomen. A key achievement for image analysis in IVM is automation for motion artefact removal [55,56]. This includes triggering imaging at specific time periods to coincide with the heartbeat or respiration, or triggering heart contractions to coincide with image acquisition. Conversely, various pieces of software have been generated for image analysis, which allows correction of sample motion following image acquisition [57]. These methods are applicable to different laser-scanning modalities, including confocal and multiphoton microscopy.

Optical Projection Tomography and Light Sheet Fluorescence Microscopy

Photon scattering in tissues hinders imaging at depths exceeding a few hundred micrometres *in vivo*, making imaging of whole organs impossible. Hence, imaging at depth requires the physical sectioning of tissues due to photon scattering. The imaging limit of conventional microscopy in terms of penetration depth is set by a physical parameter of photons known as the mean free path (MFP) (reviewed in [58]). The MFP translates as the number of scattering or collision events that a photon undergoes, each of which modifies the photon's direction of travel, ultimately resulting in image blur. For widefield epifluorescence microscopy a traditional thickness for tissue sections is 10–50 μm, which ensures a high-quality image and diffraction-limited resolution. Confocal and multiphoton microscopy allow greater penetration depths of up

Glossary

Adaptive optics: an optical method whereby deformable mirrors can correct, in real time, optical effects caused by incoming wavefront distortions.
Elastography: a medical imaging method that creates a distortion in tissue, and then measures the tissue response (e.g., mechanical waves) to the original deformation.
Fluorescence lifetime: the time that a fluorophore can spend in an excited state before emitting a photon and returning to the ground state.
Fluorescence loss in photobleaching (FLIP): an imaging method whereby a fluorescently labelled region (usually a membrane) is bleached multiple times using the laser beam of a confocal microscope, to ensure that all fluorophores are bleached. Measurement of fluorophore exchange between nonbleached and bleached area over time provides information on membrane dynamics.
Fluorescence recovery after photobleaching (FRAP): an imaging method that consists of targeting a sample area with a single high-intensity illumination, resulting in the elapse of the fluorophore's fluorescence lifetime. Over time, fluorescent probes will diffuse through the sample to replace those in nonfluorescent areas, thus allowing quantification of lateral diffusion.
Förster resonance energy transfer (FRET): a mechanism of energy transfer between a donor and an acceptor chromophore. Efficiency of energy transfer is highly linked to (i) the distance between two fluorophores, (ii) the spectral overlap of donor and acceptor, and (iii) the relative orientation of donor and acceptor dipole moments.
Graded index (GRIN) lenses: lenses of different materials that reduce optical aberrations by having a refractive index gradient, and a flat surface.
Imaging windows/optical windows: surgically implanted windows that allow visualization of internal organs inside a living mouse. Windows can be acute/terminal, or chronic, allowing visualization over days–weeks.

to 0.5–1 mm. Nevertheless, to acquire a 3D image of an entire sample using confocal or multiphoton microscopy, automated methods for the digital reconstruction of thin serial sections require the acquisition of hundreds of individual sections and/or long imaging periods under high-energy illumination. This ultimately renders confocal and multiphoton techniques impractical for imaging intact, large specimens.

Mesoscopic imaging techniques, such as light-sheet fluorescence microscopy [LSFM; also known as selective plane illumination microscopy (SPIM)] and optical projection tomography (OPT), enable visualization of larger fields of view across entire organs. The prerequisite is that these organs must be transparent or optically cleared. Tissue clearance has gained significant momentum in recent years, as shown by a rising number of clearing methods which offer different advantages, despite their use being limited to fixed tissues [59–61]. Altogether, tissue-clearance methods must satisfy three basic criteria: (i) all tissues must be efficiently cleared, (ii) cellular and subcellular structures must be adequately preserved, and (iii) tissue clearance must be compatible with fluorescence detection. Current techniques include the use of organic solvents [60,62–70], water [59,71–76], and electrophoresis-based protocols [77–79]. A summary of relevant methods for tissue clearance is shown in Table 3.

Once the sample is transparent, OPT imaging is achieved via tissue transillumination and epi-illumination over multiple projections [80]. With the OPT setup, the specimen is rotated through 360° in angular steps around a single axis while being held in position for imaging (Figure 1A). Virtual sections are independently reconstructed from the acquired images using a back-projection algorithm [81]. This method allows high-resolution imaging at penetration depths of up to 15 mm [80]. As a result, high-resolution digital sections, and 3D image reconstructions of the sampled specimen's volume, can be obtained.

LSFM, by contrast, uses a thin plane of light (or light sheet), that is shaped by a cylindrical lens or a laser scanner to exclusively illuminate the focal plane of the sample at any one time and has been used extensively to image living, if small, organisms (Figure 1B) [82]. While, in conventional microscopes, illumination and detection follows the same path, the detection pathway in LSFM is rotated by 90°. Altogether, these characteristics make it a powerful tool for live-cell imaging of large samples due to its high imaging speed, reduced toxicity, and photobleaching (reviewed in [83]). 3D image formation is based on raw images being assembled after translation or rotation of the entire sample. Multiple LSFM setups have been developed, including illumination from multiple directions, enabling doubling the penetration depth [84], or combining different mesoscopic techniques, including OPTiSPIM [85], a hybrid setup which benefits from the high resolution of SPIM with the possibility to image fluorescent and nonfluorescent contrasts of OPT. The first commercial devices were made available, and an open-source, custom-built version named OpenSPIM was produced [86,87]. OPT and/or LSFM have been used to image multicellular culture models [88–91], zebrafish [92], sparse cell populations [93], the development of plants [94], living embryos, and gene mapping [80,95], as well as multiple rodent organs in health and disease conditions [63,66,96,97]. OPT and LSFM were both successfully used to obtain detailed insight of the anatomy of the flight musculature of a *Drosophila* fly, its nervous and digestive systems, and β-galactoside activity at whole-body level [98,99]. While in its origins, the application of tissue clearing and imaging was limited to rodent organs or small whole bodies (such as that of *Drosophila* flies), a build-up on previous hydrogel embedding, tissue-clearing techniques [passive clarity technique (PACT)], imaging reagents [refractive index matching solution (RIMS)], and delivery routes [perfusion-assisted agent release (PARS)] made it possible to image whole optically cleared mice [100].

Lateral resolution: the minimum distance that can be distinguished between two contiguous reflectors, perpendicular to the ultrasound beam.
Mesoscopic imaging methods: branch of imaging referring to measurements of samples of intermediate sizes (in the range of tens of micrometres to millimetres).
Microbubbles: intravenously injected materials that serve as contrast agents in ultrasound. They consist of a low-solubility complex gas surrounded by a phospholipid shell. They resonate in an ultrasound field, and generate 'signature' harmonic signals.
Optical resolution: the shortest distance between two points, within a specimen, that can be distinguished as separate entities.
Photobleaching: a process whereby the repeated cycling of a fluorophore between ground and excited states leads to molecular damage and gradual reduction in fluorescence.
Stimulated emission depletion (STED): a method in super-resolution imaging that relies on the selective deactivation of fluorophores while leaving only a small focal spot active.
Ultrasound transducer: a device that produces sound waves which interact with body tissues and produce echoes. This signal is received and used to generate a sonogram.

Table 1. Imaging Scales and Current/Potential Applications in Parasitology

Imaging method	Resolution	Penetration depth (max)	Advantages	Potentail parasitology applications in *in vivo* imaging
Electron microscopy (and combinations with fluorescence microscopy)	2–5 nm	1 μm (TEM)	Visualizes not just the fluorophore. Can now be combined with fluorescence microscopy (correlative light and electron microscopy: CLEM) and intravital imaging.	Observation of ultrastructural details of host–pathogen interactions, cells, and infection-related changes.
STED	20 nm (lateral)	100–200 μm	Enables fluorescent imaging at a nano-scale resolution.	Observation of highly resolved structures and host–parasite interactions at subcellular resolution.
IVM: Advanced fluorescence microscopy – FRET	2–10 nm	100–200 μm	Enables quantification of protein–protein interactions *in vivo.*	Monitor enzyme activities, ion changes, host–pathogen interactions, lipid changes, mechanical stress, and molecule quantifications.
IVM: Advanced fluorescence microscopy – FRAP	2–10 nm	100–200 μm	Enables quantification of lateral diffusion dynamics.	Monitor host–pathogen interactions at the subcellular level within cells harbouring intracellular parasites, for example, organelle hijacking, nutrient acquisition.
IVM: Advanced fluorescence microscopy – FLIP	200 nm	100–200 μm	Enables quantification of membrane dynamics.	Monitor host–pathogen interactions at the subcellular level, for example, intracellular parasite membrane fusion and organelle segregation during replication.
IVM: Confocal imaging	200 nm	100–200 μm	Compromise between high resolution and fast acquisition rates *in vivo*.	Monitor host–pathogen interactions at subcellular and cellular levels.
IVM: Multiphoton microscopy	400 nm	500–800 μm	The highest advantage over other methods is high penetration depth. Low background autofluorescence.	Monitoring parasite dynamics in deep organ structures.
IVM: Spinning-disc microscopy	200 nm	100–200 μm	Fast image acquisition speed *in vivo*.	Monitoring dynamics of host–pathogen interactions, membrane dynamics, tissue changes, vasculature at near real time.
OPT	20 μm	cm in cleared samples	3D reconstruction of large, optically cleared samples.	Visualizing parasite and tissue distribution, vascular changes, and systemic changes at whole-tissue and even whole-animal level.
SPIM	200–500 nm	cm in cleared samples	3D reconstruction of large, optically cleared samples. Little phototoxicity in live imaging.	Visualizing parasite and tissue distribution, vascular changes, and systemic changes at whole-tissue and even whole-animal level.
OAI	Sub-100 μm in deep tissues	cm	Images noninvasively optical absorption contrast over a wide range of spatial scales at high speed. Able to image structures and function.	Noninvasive imaging of effects of parasite presence in tissues. Visualization of vascular and metabolic changes in various organs longitudinally.
MRI	100–500 μm	Full body	Noninvasive imaging, applicable to clinics. Provides detailed information on tissue architecture, morphology, pathology.	Can be applied to organs ranging from deep organs to skin, to study parasite effects at tissue level. Functional MRI can be used to study function in tissues affected by parasite presence.
Radiography	cm	Full body	Noninvasive imaging. Provides detailed information on tissue architecture.	Applicable to study tissue diffraction properties upon infection with different parasites.
Ultrasound	Sub-100 μm in deep tissues	Full body	Noninvasive imaging, applicable to clinics. Provides detailed information on tissue architecture, morphology, pathology.	Can be applied to organs to study parasite effects at tissue level, including metabolic changes.

Table 1. (continued)

Imaging method	Resolution	Penetration depth (max)	Advantages	Potentail parasitology applications in *in vivo* imaging
CT	mm	Full body	Noninvasive 3D imaging, applicable to clinics.	Can be applied to organs to study parasite effects at tissue level.
Bioluminescence imaging	cm	Several cm	Enables whole-body imaging in a high-throughput manner. Consistent with 3Rs on animal usage.	Visualizing luminescent parasite distribution. Potential to perform BRET *in vivo* has not been explored.
PET	mm	Full body	Allows observation of metabolic processes within the body, as well as parameters such as blood flow, metabolism, and neurotransmitters.	Observation of the effects of parasitic infections on host metabolism, blood flow perturbations, or neurotransmission at a whole-body level.
SPECT	Several mm	Full body	Allows observation of metabolic processes within the body, as well as parameters such as blood flow, metabolism, and neurotransmitters.	Observation of the effects of parasitic infections on host metabolism, blood flow perturbations, or neurotransmission at a whole-body level.

In parasitology, uses have included the generation of optically cleared gut from tsetse flies (vectors of *Trypanosoma brucei*) [101] (Figure 1C) and optically transparent *Anopheles* mosquitoes (vectors of *Plasmodium*) (Figure 1D,E). Importantly, the use of **mesoscopic methods** in parasitology has remained scarce, despite their relatively easy implementation and use. The potential of these techniques to study interactions at high resolution, and high throughput, for the phenotypic characterization of parasite-induced changes in vectors, rodents, and other model organisms is high, and worth exploring and implementing in various areas of parasitology in years to come.

Bioluminescence Imaging

Photon production is achieved primarily through luminescence and fluorescence. In luminescence, the photon is the product of exothermic chemical reactions, where an enzyme (e.g., luciferase) oxidizes a substrate (e.g., luciferin), leading to photon emission. Conversely, in fluorescence the excited states are created by absorption and emission of light. The main advantage of luminescence assays is accurate quantification with high sensitivity, which can be applied in high-throughput studies, both *in vivo* and *in vitro*.

Bioluminescence imaging relies on processes occurring in nature via the generation of light by lower organisms, including beetles, bacteria, molluscs, algae, crustaceans, annelids, and coelenterates [102]. Various bioluminescent substrates have been isolated from these organisms, and their biochemical properties have been defined (Figure 2). Across parasitology research, the main bioluminescent probe used *in vivo* is firefly luciferase (reviewed in [103,104]), with *Gaussia*, NanoLuc and *Renilla* luciferase being less commonly used. Transgenic *Plasmodium* spp., *Toxoplasma* spp., *Leishmania* spp., *Trypanosoma brucei,* and *Trypanosoma cruzi* expressing bioluminescent probes have been used for investigating parasite growth and dissemination, virulence, coinfections, parasite stage-specific promoters, drug screening, and monitoring host–pathogen interactions (reviewed in [103,104]).

In recent years, an important aim has been to achieve ultrabright luminescence to detect signals with high sensitivity in deep tissues. This has been initially achieved by generating parasites expressing codon-optimized red-shifted firefly luciferases [7,105] and ultrabright luminescent probes such as NanoLuc [106,107]. Although NanoLuc luciferase has been extremely useful *in vitro* due to its bright signal [108], its performance *in vivo* is very poor due to its short emission

Table 2. Key Examples of Organs and Parasites Imaged by IVM.

	Organs/ pathogen	Central/peripheral nervous system	Skin	Lungs	Heart	Stomach/ pancreas	Liver	Spleen	Intestines	Kidneys/ bladder	Lymph nodes	Bone marrow	Adipose tissue	Placenta
Vector-borne	*Plasmodium* spp.	[1]	[5,6]	[13]	–	–	[14,15]	[19,20]	–	–	[23]	[25]	[20]	[26,27]
	Trypanosoma brucei	[2]	[7,8]	–	–	–	–	–	–	–	–	–	–	–
	Trypanosoma cruzi	–	[10,11]	–	–	–	–	–	–	–	–	–	–	–
	Onchocerca	–	–	–	–	–	–	–	–	–	–	–	–	–
	Leishmania	–	[9]	–	–	–	[16]	–	–	–	[24]	–	–	–
	Wuchereria/Brugia	–	–	–	–	–	–	–	–	–	–	–	–	–
	Schistosoma	–	[12]	–	–	–	[17]	–	–	–	–	–	–	–
	Theileria	–	–	–	–	–	–	–	–	–	–	–	–	–
	Babesia	–	–	–	–	–	–	–	–	–	–	–	–	–
Food/water/soil-borne	*Toxoplasma*	[3,4]	–	–	–	–	–	–	[21,22]	–	–	–	–	–
	Entamoeba	–	–	–	–	–	[18]	–	–	–	–	–	–	–
	Echinococcus	–	–	–	–	–	–	–	–	–	–	–	–	–
	Ascaris	–	–	–	–	–	–	–	–	–	–	–	–	–
	Ancylostoma	–	–	–	–	–	–	–	–	–	–	–	–	–
	Necator	–	–	–	–	–	–	–	–	–	–	–	–	–
	Strongyloides	–	–	–	–	–	–	–	–	–	–	–	–	–
	Paragonimus	–	–	–	–	–	–	–	–	–	–	–	–	–
	Giardia	–	–	–	–	–	–	–	–	–	–	–	–	–
	Cryptosporidium	–	–	–	–	–	–	–	–	–	–	–	–	–

Table includes key examples for each parasite and organ rather than an exhaustive coverage. Green - IVM exists; Yellow - organ relevant, but IVM never done; Grey - IVM not done.

Table 3. Tissue Clearance Methods for SPIM and OPT

Clearing method	Rationale	Advantages	Limitations	Refs
BABB (Murray's clear; Benzyl alcohol: benzyl benzoate)	Benzyl alcohol and benzyl-benzoate.	Quick tissue clearance. Successful for clearing connective tissues.	Strong quenching of fluorescence. Solutions used are toxic.	[62]
3DISCO (3D imaging of solvent-cleared organs)	Tetrahydrofluorane, dichloromethane, and dibenzyl ether.	Successfully preserves fluorescence in tissues (brain) while enabling adequate tissue clearance.	Fluorescence quenching in some tissues. Clearance not very fast.	[63]
iDISCO (immunolabelling-enabled 3D imaging of solvent-cleared organs)	Uses dibenzylether.	Enables deep antibody diffusion in large organs. Compatible with use of Alexa Fluor dyes: does not require immediate imaging as there is no diffusion over time.	Minor.	[64]
PACT (passive clarity technique), PARS and RIMS	Passive tissue clearing and immunostaining of intact organs. Uses acrylamide, bis-acrylamide, and SDS (sodium dodecyl sulfate).	Preserves fluorescence successfully. Low maintenance procedure.	Long incubation time required. Can cause aberrations in tissue morphology.	[60]
CUBIC (clear unobstructed brain-imaging cocktails and computational analysis)	Urea, N,N,N′,N′-tetrakis (2-hydroxypropyl)ethylenediamine, Triton X-100, sucrose, and 2,2′,2″-nitrilotriethanol.	Relatively fast procedure, preserves tissue morphology and fluorescence intensity. Whole-body clearance is possible via trans-cardial perfusion with reagents.	Minor.	[65,66]
RTF	Rapid clearing method based on triethanolamine and formamide.	Can render tissues transparent within hours. Is user friendly. Preserves fluorescence signal (including GFP) and tissue structure.	Minor. Not yet validated in multiple organs.	[67]
TDE (tetrachlorodiphenylethane)	Based on 2,2′-thiodiethanol, a glycol derivative often used as mounting medium.	Reported use in brain with successful clearance and fluorescence preservation.	In high concentrations, TDE quenches fluorescence, and affects cell shape.	[68,69]
Spalteholz	Benzyl alcohol, benzyl benzoate and methylsalicylate isosafrole.	Quick tissue clearance. Successful for clearing connective tissues.	Strong quenching of fluorescence. Solutions used are toxic.	[70]
SWITCH (system-wide control of interaction time and kinetic of chemicals)	SDS and custom refractive index-matching solution. Requires glutaraldehyde and thermal delipidation, followed by refractive index-matching. Increases hybrid porosity, facilitating diffusion for labelling.	Very strong and fast clearing. Allows clearing while preserving fluorescence and antigenicity across the tissue. Buffer allows chemical reactions between exogenous and endogenous molecules. Suitable for multiplexed proteomic imaging.	Can introduce colouration artefacts.	[71]
Sca*l*eA2/U2	Urea, glycerol, and Triton X-100	Glycerol counter-balances urea-induced tissue expansion. Allows targeting lipophilic tissue regions.	Slow clearance rates. Aberrations can be introduced due to reagents used, including tissue fragility and volume enlargement of specimens. Not good in heavily myelinated tissues.	[72]
Sca*l*eS	Optimized Sca*l*e protocol. Sorbitol-based.	Preserves tissue morphology and fluorescence. Sorbitol is effective at clearing tissues otherwise difficult to clear. Allows imaging at high resolution and significant depth.	Not all tissues are successfully cleared using this method. As Sca*l*e A2/U2, not so successful in heavily myelinated tissues.	[59]
FRUIT	SeeDB-derived method that uses D (–)-fructose and urea.	Water-soluble method has additive clearance effects. Allows arterial perfusion for enhanced clearance. Compatible with yellow fluorescence	Minor. Usefulness not yet reported in multiple tissue types.	[73]

Table 3. (continued)

Clearing method	Rationale	Advantages	Limitations	Refs
		proteins. Compatible with use of lipophilic tracers.		
Clear^{T}	Based on formamide.	Since it does not use detergents or solvents, allows the use of lipophilic dyes and fluorescent tracers. Clearing speed of some tissues.	The main component is toxic. Insufficient tissue transparency for full volume imaging. Quenches fluorescence, especially GFP.	[74]
Clear^{T2}	Based on formamide and polyethylene glycol (PEG).	Allows the use of lipophilic dyes and fluorescent tracers. Clearing speed of some tissues. PEG stabilizes protein conformation, thus inhibits GFP quenching.	Insufficient tissue transparency for full-volume imaging.	[75]
SeeDB (See Deep Brain)	Combination of fructose and α-thioglycerol.	Fast clearing with optimal preservation of tissue integrity and fluorescence signal. Allows large-scale imaging.	Viscosity of saturated fructose is very high. Difficult to permeate organs. Arterial perfusion not possible.	[76]
CLARITY (clear lipid-exchanged acrylamide hybridized rigid imaging compatible tissue hydrogel)	Bioelectrochemical clearing technique. Builds an acrylamide-based hydrogel hybrid from intact tissues. Uses electrophoresis, acrylamide, bis-acrylamide, and SDS.	Preserves fluorescence successfully.	Electrophoresis base can be challenging to implement. Can damage tissues or introduce artefacts.	[77,78]
MAP (magnified analysis of the proteome)	Based on CLARITY method, uses denser gel to provide the tissue with more stability.	Allows preservation of the tissue integrity while allowing successful tissue clearance. Allows linear tissue expansion, and therefore highly resolved imaging. Allows multiple rounds of immune-labelling.	Minor.	[79]

wavelength. Recently, a novel red-shifted luciferase–luciferin pair based on the coelenterazine analogue diphenylterazine (DTZ) and a NanoLuc mutant fused to a fluorescent reporter (resulting in an ultrabright probe known as Antares2), proved to be highly successful for *in vivo* imaging [109,110]. Similarly, another highly successful combination has been that of AkaLumine hydrochloride (AkaLumine-HCl – a synthetic D-luciferin analogue), which, when catalysed by firefly luciferase, generates near-infrared emission, and has favourable distribution in deep organs [111]. Random mutagenesis of firefly luciferase-based libraries led to the generation of Akaluc, which displayed high thermostability and the brightest emission when combined with AkaLumine [112]. The Akaluc/AkaLumine-HCl combination has allowed a revolutionary advance, namely visualization of single bioluminescent cells in deep tissues of freely moving animals [112].

Further technological advances in the field of bioluminescence include dual-probe reporters which allow the detection of two signals simultaneously, at different wavelengths. These have been useful in the context of characterization of different promoters expressed at different parasite life stages [113,114]. Equally, bioluminescence can be used in the context of bioluminescence energy transfer (BRET), or hybrid biosensors (BRET–FRET, or hyBRET) for investigation of protein–protein interactions, analysis of xenografts, and optogenetics, *in vivo* [115].

Optoacoustic and Ultrasound Imaging

All optical imaging techniques mentioned above have been shown to image biological structures with potential subcellular resolution (in the range of the wavelength used) and remarkable

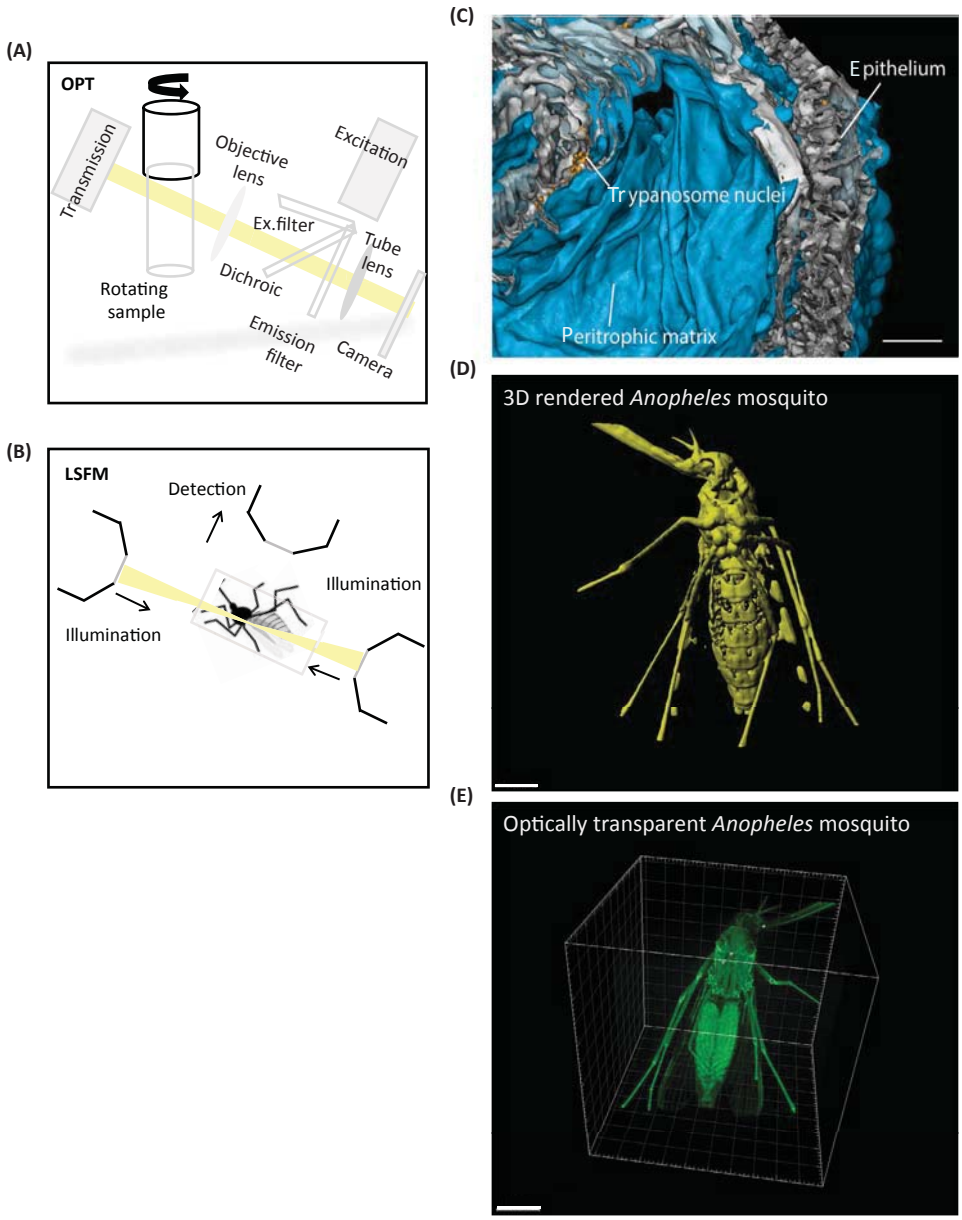

Trends in Parasitology

Figure 1. Optical Projection Tomography (OPT) and Light Sheet Fluorescence Microscopy (LSFM). (A) Principle of OPT. The optically cleared specimen is embedded in agarose, attached to a metallic cylinder within a rotating stage, and suspended in an index-matching liquid to reduce scattering and heterogeneities of refractive index throughout the specimen. When the specimen is rotated to a series of angular positions, images are captured at each orientation. The setup is aligned to ensure that the axis of rotation is perpendicular to the optical axis, so that straight-line projections going through the sample can be generated, and collected by pixels on the charge-coupled device of the camera. (B) Principle of light-sheet fluorescence microscopy (LSFM). The optically cleared sample is embedded in agarose and suspended within a sample holder inside an index-matching liquid. A thin (nm–μm) slice of the sample is illuminated perpendicularly to the direction of observation. Scanning is performed using a plane of light, which allows very fast image acquisition. (C) Surface rendering model of isolated infected fly gut. The intestinal tissue is visualized by autofluorescence (grey). The PM is stained with rhodamine-labelled WGA (cyan) and the trypanosome nucleus with a GFP-reporter (yellow).

(Figure legend continued on the bottom of the next page.)

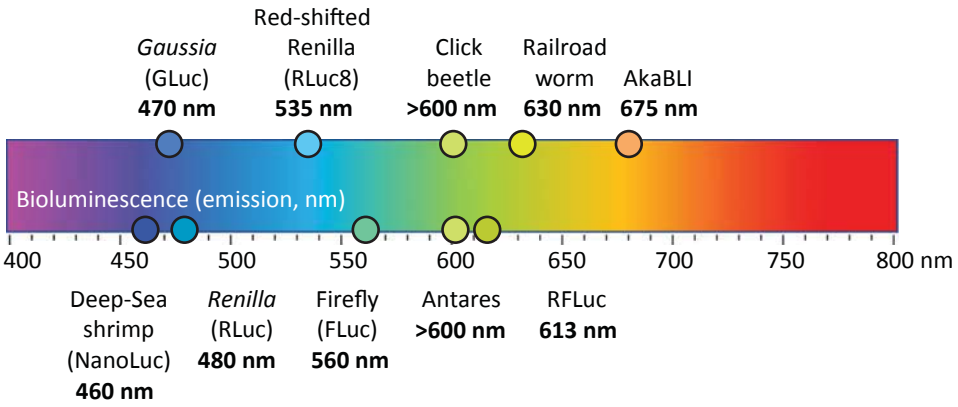

Figure 2. Bioluminescence Imaging Probes. Bioluminescence probes commonly used in *in vivo* imaging include *Gaussia* luciferase, NanoLuc, *Renilla* luciferase, click beetle luciferase (and its red- and green-shifted forms), red-shifted firefly luciferases, railroad worm luciferases, and novel probes with bright luminescence to image deep into tissues such as AkaBLI and Antares/Antares2. Isolated from different organisms, these probes have a varied range of molecular weights and maximum peak of emission wavelengths as schematically illustrated here, allowing for dual luminescence systems to be used.

contrast but are limited by strong light scattering in tissue. Optoacoustic (OA) imaging, also referred to as photoacoustic imaging, offers the ability to not only overcome this limitation but to provide structural, functional, metabolic, and even molecular information [116,117]. OA is a hybrid imaging modality, combining optics and acoustics via the thermoelastic effect [118,119]. The thermoelastic effect converts optically absorbed energy into acoustic waves, which are recorded at the tissue surface by means of ultrasound detection. Optical absorption provides the imaging contrast for OA, which means that any chromophore or molecule that selectively absorbs the illumination wavelength can be imaged [120]. Chromophores can be endogenous or exogenous. Via their spectral fingerprint, endogenous chromophores – such as haemoglobin – provide quantitative and physiological information of the vasculature. Exogenous chromophores – such as antibodies functionalized by absorbing metallic nanoparticles or dyes – are suitable for the assessment of tumours and other pathologies. These features make OA imaging an interesting technique for studying host–parasite interactions.

Imaging can be performed both in a tomographic macroscopic setup, visualizing the whole animal, or in a microscopic setup. Tomography uses an array of ultrasound sensors, often partially or completely surrounding the target, to achieve axial image resolution of typically a few hundred micrometres, determined by the bandwidth of the **ultrasound transducer**, and imaging depths of up to few centimetres [121]. By contrast, microscopy setups use a single mechanically scanned focused transducer (Figure 3A) or a tightly focused diffraction-limited laser beam to generate an image. In the former case, termed acoustic resolution microscopy, the **lateral resolution** is given by the properties of the acoustic lens and the ultrasound transducer (~40 μm at 50 MHz transducer frequency). In this configuration, OA microscopy has been shown to resolve fine structures in the dermis and assess dermal papillae [122]. It has

Scale bar: 50 μm. Figure reproduced, with permission, from [101]. (D) 3D reconstruction and rendering of a female *Anopheles* mosquito clearly showing abdominal segments, thorax, and head features. Scale bar: 70 μm. (E) 3D reconstruction and clear view of all body cavities of an optically cleared *Anopheles* mosquito. Scale bar: 100 μm. Abbreviations: PM, peritrophic matrix; WGA, wheat germ agglutinin.

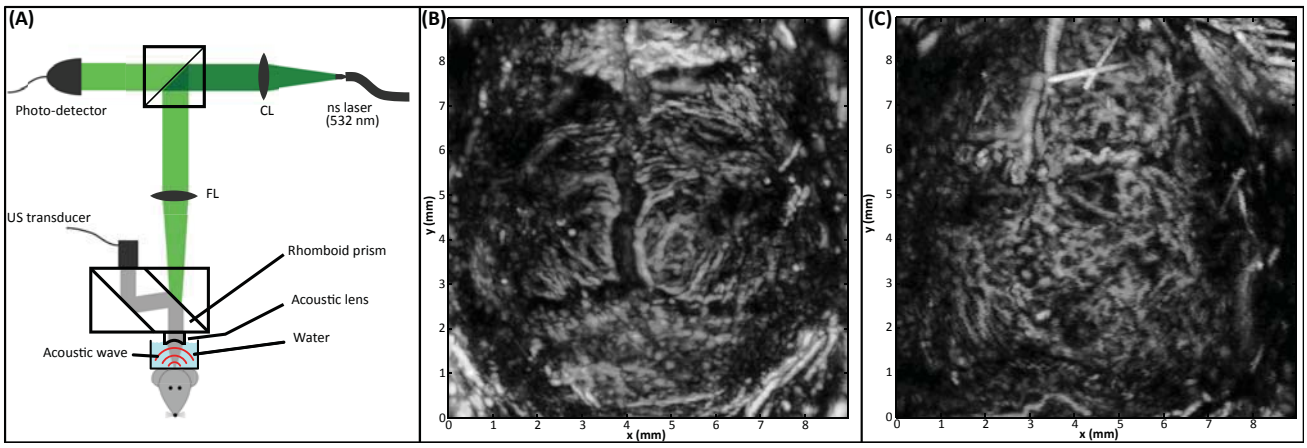

Trends in Parasitology

Figure 3. Optoacoustic Microscopy Setup and Imaging of the Brain. (A) Optoacoustic (OA) microscopy setup (acoustical resolution). The laser illumination induces thermoelastic pressure waves in the sample and triggers signal acquisition (photodetector). The generated pressure wave (red) is collected by the acoustic lens and directed to the ultrasound transducer. (B) OA microscopic image of the brain of a healthy mouse shows clearly distinguishable hemispheres. (C) The same image of a mouse infected with *Plasmodium* (5 days after infection) shows aberrant structure of the vasculature.

also been used to visualize the cerebral vascular anatomy in mice up to a depth of 3.7 mm at sub-millimetre resolution (sub-100 μm at 1 mm depth), greatly surpassing what can be achieved with purely optical techniques [123]. In the latter case, called **optical resolution** microscopy, the lateral resolution is determined by the focal spot of the laser, and imaging depth is limited by optical scattering to a maximum of 1 mm, as it is in the case of pure optical microscopy [121,124]. In low-scattering tissue, such as that found in mouse ears, the resolution can be pushed to 2.5 μm at a depth of 150 μm [125].

Both contrast and penetration depth are affected by the choice of excitation wavelength. Shorter wavelengths (typically no shorter than 532 nm) are strongly absorbed by haemoglobin and thus higher contrast can be achieved, at the expense of penetration depth. For longer wavelengths (typically up to 1300 nm), penetration depth is increased at the expense of contrast. Since the propagation speed of ultrasound waves in biological tissue is comparatively low, depth information is obtained by recording the pressure wave in a time-resolved manner. Thus, all OA imaging techniques have the potential to record three-dimensional images. Furthermore, differences in the wavelength-dependent absorption coefficients of oxygenated and deoxygenated haemoglobin can be utilized for oxygenation measurements in both tomographic [126] and microscopic [123,125] setups.

Currently, only a few commercially available *in vivo* whole-animal OA imaging devices are capable of capturing single cross-sectional tomographic images of living small animals with estimated in-plane resolutions of ~150 μm [127–129]. OA imaging has also been combined with echo-ultrasound imaging in a whole-body live mouse tomography system, with reported in-plane spatial resolutions of 150 μm (OA) and 350 μm (ultrasound) [130].

Using acoustic resolution OA microscopy (Figure 3A), we have imaged the brain of mice aged 4–6 weeks infected with *Plasmodium*. The mice had their scalp removed (the skull was left intact) prior to imaging and were kept under anaesthesia during imaging. We have found that images of healthy mice (Figure 3B) show clearly discernible hemispheres and cerebellum, while

in infected mice (5 days after infection) the major vascular landmarks could hardly be identified. The vasculature showed a large number of aberrantly distributed screw-like blood vessels, and the two hemispheres could no longer be distinguished (Figure 3C). In later stages of the disease (7+ days after infection), a significant decrease in optoacoustic signal amplitude was detected, possibly due to progressive anaemia.

Altogether, OA imaging, which combines high contrast and spectral sensitivity with the high spatial resolution obtained in ultrasound imaging, provides excellent visualization of microvasculature, making it a powerful tool for basic parasitological research and preclinical applications. Combined with exogenous optically absorbing agents or genetically expressed reporters it has been proven to provide molecular information with high sensitivity and specificity.

Ultrasound imaging itself has also been successfully used in the field of parasitology and in medical imaging. Ultrasound uses high-frequency sound waves, which are reflected off body structures, rendering an image. Key advances in ultrasound over the past decade include **elastography** [131], ultrasound contrast agent imaging using **microbubbles** (reviewed in [132]), super-resolution imaging, 2D array transducer, and ultrafast ultrasound imaging [133]. While these advances have been widely explored in other fields of research, they remain to be used in *in vivo* parasitology, and have enormous potential. Elastography is a technique referred to as 'palpating by imaging', enabling measurement and visualization of tissue mechanical properties in health and disease. In terms of contrast agents, microbubbles provide considerable advantages to ultrasound imaging, including the possibility of studying blood rheology and tissue perfusion, and of enhancing vascular permeability, drug and gene delivery, and local heating (reviewed in [134]). Finally, ultrafast and super-resolution ultrasound imaging were achieved using intravenous injection of microbubbles, the properties of which allowed haemodynamic quantification and imaging structures at 10 mm under the cranium. Single echoes from individual microbubbles could be detected, allowing accurate quantification of blood flow speeds at an imaging rate of 1000 frames per second [133]. Altogether, technological improvements in ultrasound speed and resolution, as well as echosonography applications, hold enormous potential for parasitology in terms of studying changes in rheology, vascular permeability, tissue perfusion, and changes in the physiology of important structures such as the brain–blood barrier.

Magnetic Resonance Imaging

Magnetic resonance imaging (MRI) is a noninvasive imaging technique uniquely suited to image deep inside tissue with high spatial resolution and without ionizing radiation. MRI is based on the magnetic properties of protons and neutrons within atomic nuclei of the body, particularly of hydrogen, as water is a major component of the human body. The spin of hydrogen nuclei can be measured as they show an uneven number of protons. Therefore, after placing the body inside the magnetic field of the MRI scanner, the spins start to process with the Lamour frequency and align with the magnetic field (in both directions, however slightly more in the field direction). Upon application of a radiofrequency (RF) pulse with exactly the same Lamour frequency, the nuclei can absorb energy and transition from lower to higher energy states (so called spin excitation). After the RF pulse is switched off, the nuclei return to their equilibrium state. This process requires time and depends on the surrounding tissue (also known as relaxation time). During the relaxation process, a signal can be detected by RF coils in the scanner, which can be reconstructed by advanced imaging techniques to an image of the human body (reviewed in [135]). MRI offers extraordinary advantages, including high spatial resolution, and the opportunity of simultaneously extracting physiological, molecular, and

anatomical information from the body. Conversely, its limitations include low sensitivity, long scanning time, and probe quantity required for imaging.

MRI has improved our understanding of diseases in parasitology by detecting pathological alterations, for example, in the brain, caused by *Toxoplasma* [136] (Figure 4A), *Trypanosoma brucei* [137] (Figure 4B), and *Plasmodium* [138] (Figure 4C, courtesy of Angelika Hoffmann). In this section we discuss the advances in the technique relevant to parasitology, in three specific aspects: MRI probes, multimodal mesoscopic imaging, and the uses of functional MRI to address translational questions.

Contrast agents are exogenous compounds administered to improve the image contrast and detect pathological alterations more accurately. Significant efforts have been made to improve MRI by developing contrast agents for use as probes and sensors. These include gadolinium agents (Gd^{3+}) and derivatives including gadolinium hexanedione [139], gadofluorine and liposomal-based gadolinium nanoparticles [140]. These contrast agents are used, for example, in the study of brain nerve barrier permeability [141], blood-vessel remodelling [142], or cellular uptake. Other agents include manganese-based agents such as manganese chloride ($MnCl_2$) [143], manganese oxide (MnO) [144], and silica-coated particles, which allow detection of

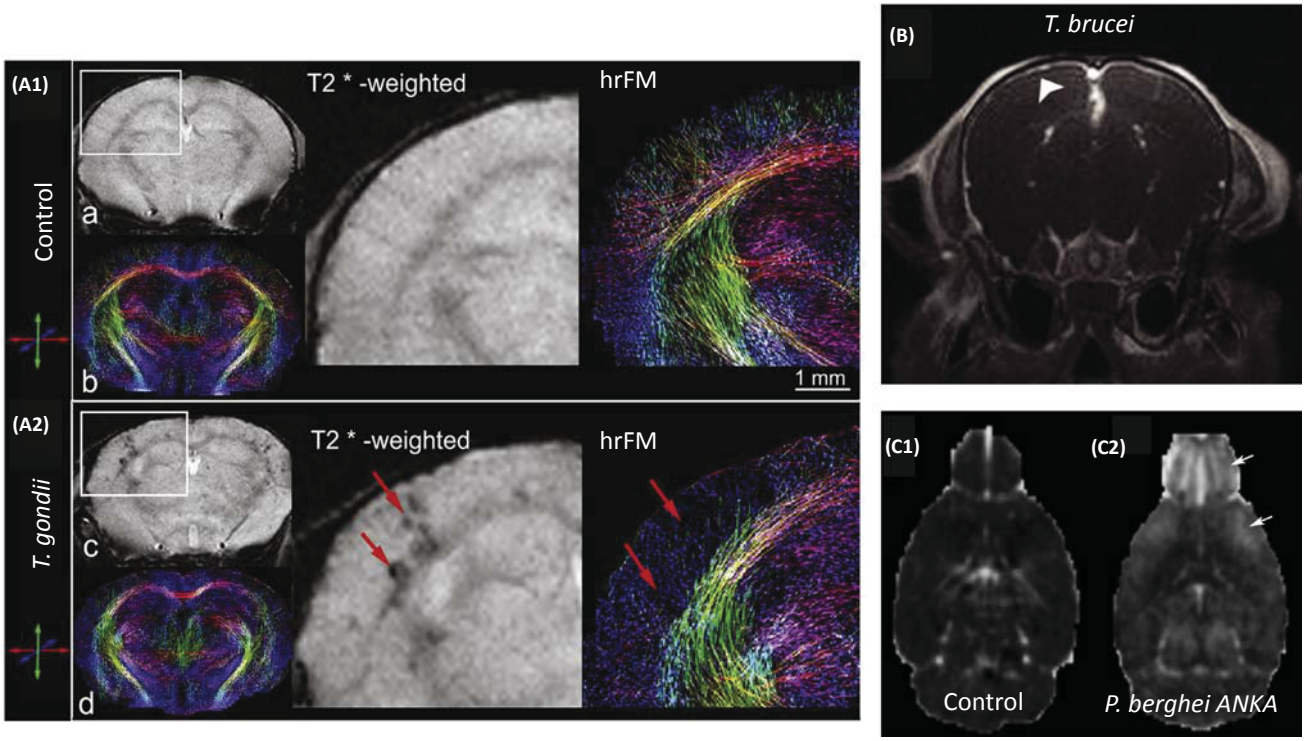

Trends in Parasitology

Figure 4. Magnetic Resonance Imaging (MRI) of the Brain. (A) T2*-weighted images and high-resolution fibre maps of (A1) uninfected and (A2) *Toxoplasma gondii*-infected mouse brains. Arrows in infected brains show injuries in the somatosensory cortex (T2*-weighted images), and affected fibre density and cortical connectivity pattern (hrFM images). Figure reproduced, with permission, from [136]. (B) MRI scan of a mouse at 28 days postinfection with *Trypanosoma brucei*, following administration of contrast. Arrowhead shows meningeal enhancement of the hind-most section of the brain. Figure reproduced, with permission, from [137]. (C) T1 subtraction maps to illustrate blood–brain barrier (BBB) disruption with rostral predominance in a *Plasmodium*-infected mouse (C1) compared to a mouse not displaying BBB disruption (C2) (courtesy of Angelika Hoffmann).

specific cell populations *in vivo* either on their own, or by combining with other contrast agents. Equally, paramagnetic iron oxide (SPIO) agents, perfluorocarbons (PFCs), and highly-shifted proton MRI [145–147], have been particularly useful for sensitively tracking and visualizing cell homing *in vivo*[148–150]. Altogether, advances in MRI contrast agents and probes have allowed the monitoring of cell functions, including enzymatic activity, gene expression, and death, as well as sensitive tracking of cell populations (reviewed in [151]).

While the output of MRI is imaging of anatomical changes, functional MRI (fMRI) is based on allowing visualization of metabolic function by tissues. fMRI allows measurement of blood flow

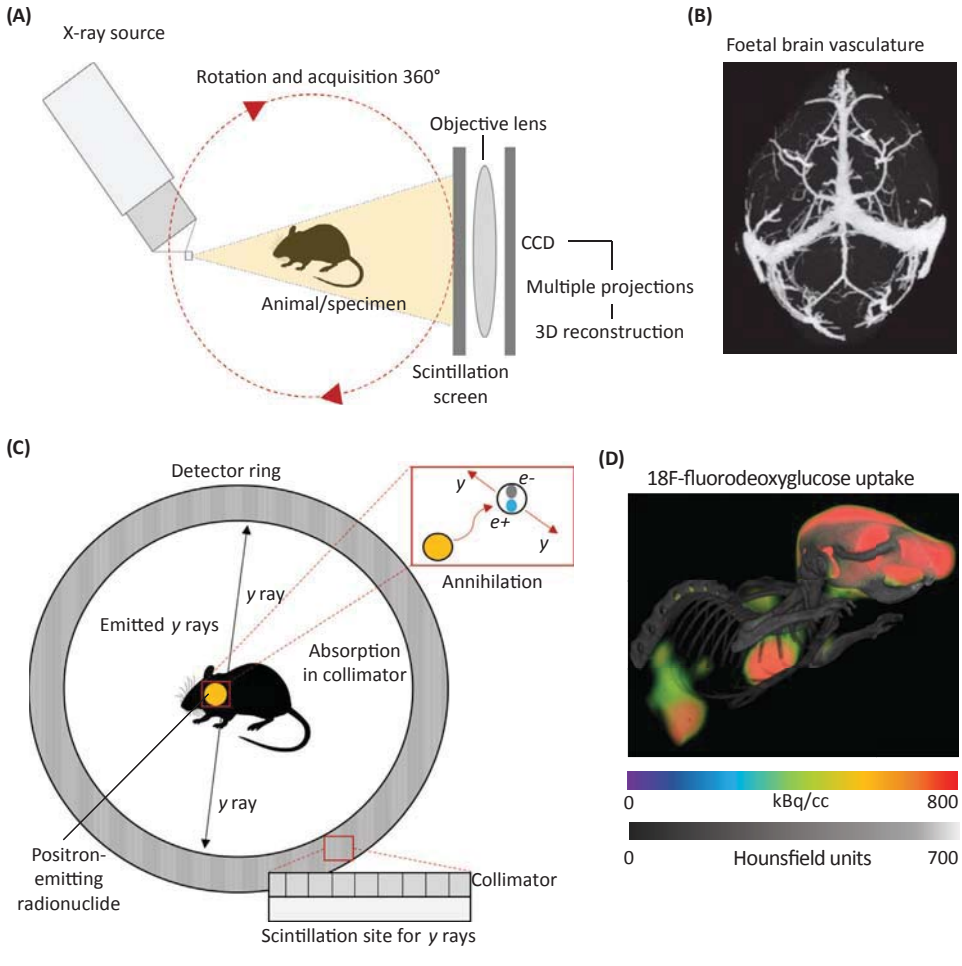

Trends in Parasitology

Figure 5. X-Ray-Based and Positron Emission Tomography (PET)-Based Imaging. (A) Principal components of a microcomputer tomography scanner include an X-ray source that produces X-rays which travel through the sample and are collected on the other side by an X-ray detector (scintillation screen, lens, and charge-coupled device camera). Rotation of the X-ray source and detector allows acquisition over 360°, allowing the generation of a series of projection images. These images can be processed to produce a 3D image of the specimen. (B) Maximum-intensity projection from an X-ray micro-computed tomography (micro-CT) study of the brain vasculature of foetuses from malaria-infected rodent mothers. The brain vasculature shown is that of a foetus from an uninfected mouse. Figure adapted from [154]. (C) Radioactive tracers are injected into the mouse and will emit positrons by radioactive decay. Upon decay, positrons are released from the nucleus of the radionuclide and annihilate with electrons in the tissue, releasing gamma-photons that can be detected within a coincidence detector ring (composed of a collimator and scintillation crystals). This allows mapping the anatomical localization of the tracer. (D) 3D reconstruction of a mouse imaged by PET-CT in a study investigating glucose uptake during the dark phase of a 24 h light–dark cycle. (18)F-fluorodeoxyglucose (FDG) was used as a tracer, and shows highest accumulation in the brain, heart, and bladder, followed by the kidneys and brown adipose tissue. Scale bars represent CT intensity (grey scale), and FDG uptake (colour scale, radioactivity per tissue volume). Figure adapted from [155].

changes, or blood oxygen level fluctuations, providing a picture of oxygen consumption. It is based on the use of blood-oxygen-level-dependent (BOLD) contrast, based on increased or decreased concentrations of paramagnetic deoxyhaemoglobin associated with changes in neuronal activity (reviewed in [152]). The use of this technique has been relatively scarce in parasitology, yet it has potential for a wide number of parasites, which induce metabolic and/or functional changes in tissues. Similarly, the generation of MRI scanners such as the 9.4 T equipment [153] offers improved imaging resolution.

X-Ray-Based and Gamma-Ray-Based Noninvasive Imaging Methods

Other imaging methods which have relevant clinical translation potential include radiography, computed tomography, X-ray micro-CT (Figure 5A,B) [154], and radioisotope-based imaging such as SPECT and PET (Figure 5C,D) [155].

Two categories of X-ray-based imaging are structural and functional imaging, enabling studies of anatomical structures and of changes in biological functions such as metabolism, blood flow, and biochemical composition of tissues, respectively. Functional analysis of tissues and their composition using X-rays has seen progress with the use of exogenous contrast agents, and is based on the possible interactions between X-rays and matter. These include X-ray attenuation, X-ray fluorescence, and X-ray-excited optical luminescence (reviewed in [156,157]).

Equally noninvasive is imaging based on gamma-ray emission from radioisotope-labelled biomolecules within samples upon radioactive decay, namely PET and SPECT. In both methods, radioactive biomolecules, synthesized from radio-nucleotides, are administered, and, following biological interactions in specific tissues, there is decay, resulting in the emission of gamma photons. These photons can be detected by PET and SPECT scanners and can be tomographically reconstructed to generate 3D images of functional tissue activity [158] (Figure 5C,D). The use of radiography-based and nuclear-imaging-based methods has been relatively limited in parasitology, yet has potential for the study of host–pathogen interaction effects on organ functions, tissue composition, and metabolic changes upon infection.

Concluding Remarks

Altogether, multiple methods for *in vivo* imaging as stand-alone techniques have allowed improved resolution (e.g., advanced microscopy methods such as super-resolution with IVM), decreased invasiveness (e.g., by the use of OAI), increased penetration depth allowing for imaging of organ regions previously impossible to observe *in vivo* (e.g., through the use of GRIN lenses for IVM), and functional imaging with high resolution (e.g., fMRI, MRI, PET, SPECT). Many of these techniques have successfully reached the parasitology field, particularly IVM. However, the advances in IVM methods and other techniques altogether, still hold enormous potential and applicability, which need to be explored (see Outstanding Questions). For instance, these advances open up the possibility to image the heart upon infection with *T. cruzi,* the digestive organs upon infection with *T. gondii,* and deep-brain structures upon infection with *T. brucei*. Functional MRI and advances in X-ray-based and gamma-ray-based methods could enable the study of functional and anatomical changes in tissues and organs upon infection, as well as fluid dynamics such as blood flow. Aside from these advances in stand-alone platforms, equally relevant will be the use of hybrid, multi-modality systems which could provide interesting opportunities to study host–pathogen interactions *in vivo* at various levels simultaneously.

Acknowledgments

We are grateful to Volker Heussler (IZB, University of Bern) for helpful advice and intellectual input on the techniques relevant to OPT, LSFM, and OAI, and training and discussions key to these methods, and IVM. We thank also the MIC at

Outstanding Questions

Can the parasitology field take advantage of motion-correction mechanisms to study parasites in the heart or gut by IVM?

IVM, OPT, SPIM, and MRI allow access to the gastrointestinal system. What can these techniques teach us in the context of food-borne and water-borne parasites?

Can new improvements in IVM applications, allowing visualization of deeper organ structures, enable the imaging of rare infection events such as *T. brucei* and *T. gondii* crossing the blood–brain barrier?

How can OPT and SPIM be modified to study the impact of parasites on vector biology, and host–pathogen interactions within vector hosts?

Can OPT, SPIM, and other relevant hybrid platforms, help to address questions relevant to parasite dynamics and spread?

Will MRI and OAI, as well as hybrid imaging platforms, enable us to address questions relevant to metabolic dysregulation by parasitic infections?

How can technological advances in imaging methods, applied to animal models, be better translated to human medicine in the context of parasitology?

Can experiments be repeated frequently enough to generate robust statistics?

the University of Bern, for providing access and training in all relevant imaging methods hereby discussed. We thank Federica Moalli, Renzo Danuser (TKI, Bern); Emmanuel G. Reynaud (University College, Dublin) and Jessica Kehrer (Centre for Infectious Diseases, Heidelberg University Hospital) for helpful input for OPT and LSFM techniques and discussions. We thank Robert Nuster (IAP, Bern) for experimental help during the establishment of OAI for experimental cerebral malaria imaging. We are grateful to Angelika Hoffmann (Department of Neuroradiology, Heidelberg University Hospital) for her helpful input on MRI techniques, for kindly providing Figure 4C (MRI of a Plasmodium-infected brain), and for carefully proofreading this manuscript's sections relevant to MRI. MDN is funded by EMBO fellowship ALTF 1048-2016, and by EVIMalaR (242095 FP7) and RSHTM (000529) fellowships with Volker Heussler (IZB, Bern) related to OPT and OAI studies, as well as Swiss National Science Foundation fellowships 310030_159519 and 316030_145013 funding work carried out in his laboratory. FS and MF acknowledge the financial support of the Swiss National Science Foundation (No: 205320_179038/1). Work in the laboratory of FF is funded by a Human Frontier Science Program grant (RGY 0066) and the German Science Foundation (SFB 1129). We apologize to the many colleagues for not citing their work due to restrictions by the journal and the broad scope of the review.

References

1. Nacer, A. *et al.* (2014) Experimental cerebral malaria pathogenesis – hemodynamics at the blood brain barrier. *PLoS Pathog.* 10, e1004528
2. Coles, J.A. *et al.* (2015) Intravital imaging of a massive lymphocyte response in the cortical dura of mice after peripheral infection by trypanosomes. *PLoS Negl. Trop. Dis.* 9, e0003714
3. Konradt, C. *et al.* (2016) Endothelial cells are a replicative niche for entry of *Toxoplasma gondii* to the central nervous system. *Nat. Microbiol.* 1, 16001
4. Estato, V. *et al.* (2018) The neurotropic parasite *Toxoplasma gondii* induces sustained neuroinflammation with microvascular dysfunction in infected mice. *Am. J. Pathol.* 188, 2674–2687
5. Amino, R. *et al.* (2006) Quantitative imaging of *Plasmodium* transmission from mosquito to mammal. *Nat. Med.* 12, 220–224
6. Hopp, C.S. *et al.* (2015) Longitudinal analysis of *Plasmodium* sporozoite motility in the dermis reveals component of blood vessel recognition. *eLife* 4, e07789
7. Calvo-Alvarez, E. *et al.* (2018) A new chimeric triple reporter fusion protein as a tool for *in vitro* and *in vivo* multimodal imaging to monitor the development of African trypanosomes and *Leishmania* parasites. *Infect. Genet. Evol.* 63, 391–403
8. Capewell, P. *et al.* (2016) The skin is a significant but overlooked anatomical reservoir for vector-borne African trypanosomes. *eLife* 5, e17716
9. Peters, N.C. *et al.* (2008) *In vivo* imaging reveals an essential role for neutrophils in leishmaniasis transmitted by sand flies. *Science* 321, 970–974
10. Soares, A.C. *et al.* (2014) Intravital microscopy and image analysis of Rhodnius prolixus (Hemiptera: Reduviidae) hematophagy: the challenge of blood intake from mouse skin. *Parasitol. Int.* 63, 229–236
11. Soares, A.C. *et al.* (2006) Salivation pattern of Rhodnius prolixus (Reduviidae; Triatominae) in mouse skin. *J. Insect Physiol.* 52, 468–472
12. Paveley, R.A. *et al.* (2009) Fluorescent imaging of antigen released by a skin-invading helminth reveals differential uptake and activation profiles by antigen presenting cells. *PLoS Negl. Trop. Dis.* 3, e528
13. Frevert, U. *et al.* (2014) Imaging Plasmodium immunobiology in liver, brain, and lung. *Parasitol. Int.* 63, 171–186
14. Tavares, J. *et al.* (2013) Role of host cell traversal by the malaria sporozoite during liver infection. *J. Exp. Med.* 210, 905–915
15. Sturm, A. *et al.* (2006) Manipulation of host hepatocytes by the malaria parasite for delivery into liver sinusoids. *Science* 313, 1287–1290
16. Beattie, L. *et al.* (2010) Dynamic imaging of experimental Leishmania donovani-induced hepatic granulomas detects Kupffer cell-restricted antigen presentation to antigen-specific $CD8^+$ T cells. *PLoS Pathog.* 6, e1000805
17. Girgis, N.M. *et al.* (2014) Ly6Chigh monocytes become alternatively activated macrophages in schistosome granulomas with help from $CD4^+$ cells. *PLoS Pathog.* 10, e1004080
18. Coudrier, E. *et al.* (2004) Myosin II and the Gal-GalNAc lectin play a crucial role in tissue invasion by Entamoeba histolytica. *Cell Microbiol.* 7, 19–27
19. Martin-Jaular, L. *et al.* (2011) Strain-specific spleen remodelling in *Plasmodium yoelii* infections in Balb/c mice facilitates adherence and spleen macrophage-clearance escape. *Cell Microbiol.* 13, 109–122
20. De Niz, M. *et al.* (2016) The machinery underlying malaria parasite virulence is conserved between rodent and human malaria parasites. *Nat. Commun.* 7, 11659
21. Coombes, J.L. *et al.* (2013) Motile invaded neutrophils in the small intestine of *Toxoplasma gondii*-infected mice reveal a potential mechanism for parasite spread. *Proc. Natl. Acad. Sci. U. S. A.* 110, E1913–E1922
22. da S. Watanabe, P. *et al.* (2018) Immunocompetent host develops mild intestinal inflammation in acute infection with *Toxoplasma gondii*. *PLoS One* 13, e0190155–e0190155
23. Radtke, A.J. *et al.* (2015) Lymph-node resident $CD8^+$ dendritic cells capture antigens from migratory malaria sporozoites and induce $CD8^+$ T cell responses. *PLoS Pathog.* 11, e1004637
24. Bajénoff, M. *et al.* (2006) Natural killer cell behavior in lymph nodes revealed by static and real-time imaging. *J. Exp. Med.* 203, 619–631
25. De Niz, M. *et al.* (2018) *Plasmodium* gametocytes display homing and vascular transmigration in the host bone marrow. *Sci. Adv.* 4, eaat3775
26. de Moraes, L.V. *et al.* (2013) Intravital placenta imaging reveals microcirculatory dynamics impact on sequestration and phagocytosis of Plasmodium-infected erythrocytes. *PLoS Pathog.* 9, e1003154
27. Lima, F.A. *et al.* (2014) Intravital microscopy technique to study parasite dynamics in the labyrinth layer of the mouse placenta. *Parasitol. Int.* 63, 254–259
28. Lagerweij, T. *et al.* (2017) Optical clearing and fluorescence deep-tissue imaging for 3D quantitative analysis of the brain tumor microenvironment. *Angiogenesis* 20, 533–546
29. Schuh, C.D. *et al.* (2016) Long wavelength multiphoton excitation is advantageous for intravital kidney imaging. *Kidney Int.* 89, 712–719
30. Friedl, P. *et al.* (2007) Biological second and third harmonic generation microscopy. *Curr. Protoc. Cell Biol.* 34, 4.15.1–4.15.21
31. Perillo, E.P. *et al.* (2016) Deep *in vivo* two-photon microscopy with a low cost custom built mode-locked 1060 nm fiber laser. *Biomed. Opt. Express* 7, 324–334
32. Michalet, X. *et al.* (2005) Quantum dots for live cells, *in vivo* imaging, and diagnostics. *Science* 307, 538–544

33. Zhao, J. *et al.* (2018) Recent developments in multimodality fluorescence imaging probes. *Acta Pharm. Sin. B* 8, 320–338
34. Nobis, M. *et al.* (2018) Molecular mobility and activity in an intravital imaging setting —implications for cancer progression and targeting. *J. Cell Sci.* 131, jcs206995
35. Radbruch, H. *et al.* (2015) Intravital FRET: probing cellular and tissue function *in vivo*. *Int. J. Mol. Sci.* 16, 11713–11727
36. Komatsu, N. *et al.* (2011) Development of an optimized backbone of FRET biosensors for kinases and GTPases. *Mol. Biol. Cell* 22, 4647–4656
37. Hires, S.A. *et al.* (2008) Reporting neural activity with genetically encoded calcium indicators. *Brain Cell Biol.* 36, 69–86
38. Tretiakova, D.S. *et al.* (2018) Lateral stress profile and fluorescent lipid probes: FRET pair of probes that introduces minimal distortions into lipid packing. *Biochim. Biophys. Acta – Biomembr.* 1860, 2337–2347
39. Kinoshita, M. *et al.* (2017) Emphatic visualization of sphingomyelin-rich domains by inter-lipid FRET imaging using fluorescent sphingomyelins. *Sci. Rep.* 7, 16801
40. Dai, T. *et al.* (2018) Liposomes and lipid disks traverse the BBB and BBTB as intact forms as revealed by two-step Förster resonance energy transfer imaging. *Acta Pharm. Sin. B* 8, 261–271
41. Hirata, E. and Kiyokawa, E. (2016) Future perspective of single-molecule FRET biosensors and intravital FRET microscopy. *Biophys. J.* 111, 1103–1111
42. Welf, E.S. *et al.* (2016) Quantitative multiscale cell imaging in controlled 3D microenvironments. *Dev. Cell* 36, 462–475
43. Woehler, A. (2013) Simultaneous quantitative live cell imaging of multiple FRET-based biosensors. *PLoS One* 8, e61096
44. Erami, Z. *et al.* (2016) Intravital FRAP imaging using an E-cadherin-GFP mouse reveals disease- and drug-dependent dynamic regulation of cell-cell junctions in live tissue. *Cell Rep.* 14, 152–167
45. Machado, M.J.C. and Mitchell, C.A. (2011) Temporal changes in microvessel leakiness during wound healing discriminated by *in vivo* fluorescence recovery after photobleaching. *J. Physiol.* 589, 4681–4696
46. de Grauw, C.J. *et al.* (1999) Imaging properties in two-photon excitation microscopy and effects of refractive-index mismatch in thick specimens. *Appl. Opt.* 38, 5995
47. Andresen, V. *et al.* (2012) High-resolution intravital microscopy. *PLoS One* 7, e50915
48. Wegner, W. *et al.* (2017) *In vivo* mouse and live cell STED microscopy of neuronal actin plasticity using far-red emitting fluorescent proteins. *Sci. Rep.* 7, 11781
49. White, M.D. *et al.* (2018) *In vivo* imaging of single mammalian cells in development and disease. *Trends Mol. Med.* 24, 278–293
50. Kim, J.K. *et al.* (2012) Fabrication and operation of GRIN probes for *in vivo* fluorescence cellular imaging of internal organs in small animals. *Nat. Protoc.* 7, 1456–1469
51. Barretto, R.P.J. *et al.* (2011) Time-lapse imaging of disease progression in deep brain areas using fluorescence microendoscopy. *Nat. Med.* 17, 223–229
52. Reismann, D. *et al.* (2017) Longitudinal intravital imaging of the femoral bone marrow reveals plasticity within marrow vasculature. *Nat. Commun.* 8, 2153
53. Ducourthial, G. *et al.* (2015) Development of a real-time flexible multiphoton microendoscope for label-free imaging in a live animal. *Sci. Rep.* 5, 18303
54. Rueckel, M. *et al.* (2006) Adaptive wavefront correction in two-photon microscopy using coherence-gated wavefront sensing. *Proc. Natl. Acad. Sci. U. S. A.* 103, 17137–17142
55. Lee, S. *et al.* (2014) Automated motion artifact removal for intravital microscopy, without a priori information. *Sci. Rep.* 4, 4507
56. Taylor, J.M. (2014) Optically gated beating-heart imaging. *Front. Physiol.* 5, 481
57. Warren, S.C. *et al.* (2018) Removing physiological motion from intravital and clinical functional imaging data. *eLife* 7, e35800
58. Ntziachristos, V. (2010) Going deeper than microscopy: the optical imaging frontier in biology. *Nat. Methods* 7, 603–614
59. Hama, H. *et al.* (2015) ScaleS: an optical clearing palette for biological imaging. *Nat. Neurosci.* 18, 1518–1529
60. Tomer, R. *et al.* (2014) Advanced CLARITY for rapid and high-resolution imaging of intact tissues. *Nat. Protoc.* 9, 1682–1697
61. Richardson, D.S. and Lichtman, J.W. (2016) Clarifying tissue clearing. *Cell* 162, 246–257
62. Dodt, H.-U. *et al.* (2007) Ultramicroscopy: three-dimensional visualization of neuronal networks in the whole mouse brain. *Nat. Methods* 4, 331–336
63. Ertürk, A. *et al.* (2012) Three-dimensional imaging of solvent-cleared organs using 3DISCO. *Nat. Protoc.* 7, 1983–1995
64. Renier, N. *et al.* (2014) iDISCO: a simple, rapid method to immunolabel large tissue samples for volume imaging. *Cell* 159, 896–910
65. Susaki, E.A. *et al.* (2014) Whole-brain imaging with single-cell resolution using chemical cocktails and computational analysis. *Cell* 157, 726–739
66. Abe, J. *et al.* (2016) Light sheet fluorescence microscopy for in situ cell interaction analysis in mouse lymph nodes. *J. Immunol. Methods* 431, 1–10
67. Yu, T. *et al.* (2018) RTF: a rapid and versatile tissue optical clearing method. *Sci. Rep.* 8, 1964
68. Staudt, T.I. *et al.* (2007) 2, 2′-thiodiethanol: a new water soluble mounting medium for high resolution optical microscopy. *Microsc. Res. Tech.* 70, 1–9
69. Aoyagi, Y. *et al.* (2015) A rapid optical clearing protocol using 2, 2′-thiodiethanol for microscopic observation of fixed mouse brain. *PLoS One* 10, e0116280
70. Spalteholz, W. (1914) *Über das Durchsichtigmachen von Menschlichen und Tierischen Präparaten und Seine Theoretischen Bedingungen, nebst Anhang,* Über Knochenfärbung, (Hirzel)
71. Murray, E. *et al.* (2015) Simple, scalable proteomic imaging for high-dimensional profiling of intact systems. *Cell* 163, 1500–1514
72. Hama, H. *et al.* (2011) Scale: a chemical approach for fluorescence imaging and reconstruction of transparent mouse brain. *Nat. Neurosci.* 14, 1481–1488
73. Hou, B. *et al.* (2015) Scalable and Dil-compatible optical clearance of the mammalian brain. *Front. Neuroanat.* 9, 19
74. Ikawa, M. *et al.* (2018) A rapid and non-invasive selection of transgenic embryos before implantation using green fluorescent protein (GFP). *FEBS Lett.* 375, 125–128
75. Kuwajima, T. *et al.* (2013) ClearT: a detergent- and solvent-free clearing method for neuronal and non-neuronal tissue. *Development* 140, 1364–1368
76. Ke, M.-T. *et al.* (2013) SeeDB: a simple and morphology-preserving optical clearing agent for neuronal circuit reconstruction. *Nat. Neurosci.* 16, 1154–1161
77. Chung, K. *et al.* (2013) Structural and molecular interrogation of intact biological systems. *Nature* 497, 332–337
78. Poguzhelskaya, E. *et al.* (2014) Simplified method to perform CLARITY imaging. *Mol. Neurodegener.* 9, 19
79. Ku, T. *et al.* (2016) Multiplexed and scalable super-resolution imaging of three-dimensional protein localization in size-adjustable tissues. *Nat. Biotechnol.* 34, 973–981
80. Sharpe, J. *et al.* (2002) Optical projection tomography as a tool for 3D microscopy and gene expression studies. *Science* 296, 541–545
81. Kak, A.C. and Slaney, M. (1988) *Principles of Computerized Tomographic Imaging,* IEEE Press
82. Huisken, J. *et al.* (2004) Optical sectioning deep inside live embryos by selective plane illumination microscopy. *Science* 305, 1007–1009

83. Pampaloni, F. *et al.* (2007) The third dimension bridges the gap between cell culture and live tissue. *Nat. Rev. Mol. Cell Biol.* 8, 839–845
84. Huisken, J. and Stainier, D.Y.R. (2007) Even fluorescence excitation by multidirectional selective plane illumination microscopy (mSPIM). *Opt. Lett.* 32, 2608–2610
85. Mayer, J. *et al.* (2014) OPTiSPIM: integrating optical projection tomography in light sheet microscopy extends specimen characterization to nonfluorescent contrasts. *Opt. Lett.* 39, 1053–1056
86. Pitrone, P.G. *et al.* (2013) OpenSPIM: an open-access light-sheet microscopy platform. *Nat. Methods* 10, 598–599
87. Gualda, E.J. *et al.* (2013) OpenSpinMicroscopy: an open-source integrated microscopy platform. *Nat. Methods* 10, 599
88. Jakob, P.H. *et al.* (2016) A 3-D cell culture system to study epithelia functions using microcarriers. *Cytotechnology* 68, 1813–1825
89. Pampaloni, F. *et al.* (2014) Tissue-culture light sheet fluorescence microscopy (TC-LSFM) allows long-term imaging of three-dimensional cell cultures under controlled conditions. *Integr. Biol.* 6, 988–998
90. Pampaloni, F. *et al.* (2015) Live spheroid formation recorded with light sheet-based fluorescence microscopy. In *Advanced Fluorescence Microscopy: Methods and Protocols* (Verveer, J.P., ed.), pp. 43–57, Springer
91. Pampaloni, F. *et al.* (2015) Light sheet-based fluorescence microscopy (LSFM) for the quantitative imaging of cells and tissues. *Cell Tissue Res.* 360, 129–141
92. Correia, T. *et al.* (2015) Accelerated optical projection tomography applied to *in vivo* imaging of zebrafish. *PLoS One* 10, e0136213
93. Chen, L. *et al.* (2015) Mesoscopic *in vivo* 3-D tracking of sparse cell populations using angular multiplexed optical projection tomography. *Biomed. Opt. Express* 6, 1253–1261
94. Maizel, A. *et al.* (2011) High-resolution live imaging of plant growth in near physiological bright conditions using light sheet fluorescence microscopy. *Plant J.* 68, 377–385
95. Summerhurst, K. *et al.* (2008) 3D representation of Wnt and Frizzled gene expression patterns in the mouse embryo at embryonic day 11.5 (Ts19). *Gene Expr. Patterns* 8, 331–348
96. Alves, S. *et al.* (2016) Ultramicroscopy as a novel tool to unravel the tropism of AAV gene therapy vectors in the brain. *Sci. Rep.* 6, 28272
97. Dobosz, M. *et al.* (2014) Multispectral fluorescence ultramicroscopy: three-dimensional visualization and automatic quantification of tumor morphology, drug penetration, and antiangiogenic treatment response. *Neoplasia* 16, 1–13
98. McGurk, L. *et al.* (2007) Three-dimensional imaging of *Drosophila melanogaster*. *PLoS One* 2, e834
99. Jährling, N. *et al.* (2010) Three-dimensional reconstruction and segmentation of intact drosophila by ultramicroscopy. *Front. Syst. Neurosci.* 4, 1
100. Yang, B. *et al.* (2014) Single-cell phenotyping within transparent intact tissue through whole-body clearing. *Cell* 158, 945–958
101. Schuster, S. *et al.* (2017) Developmental adaptations of trypanosome motility to the tsetse fly host environments unravel a multifaceted *in vivo* microswimmer system. *eLife* 6, e27656
102. Badr, C.E. (2014) . In *Bioluminescence Imaging: Basics and Practical Limitations BT – Bioluminescent Imaging: Methods and Protocols* (Badr, C.E., ed.), pp. 1–18, Humana Press
103. Avci, P. *et al.* (2017) *In vivo* monitoring of infectious diseases in living animals using bioluminescence imaging. *Virulence* 9, 28–63
104. Siciliano, G. and Alano, P. (2015) Enlightening the malaria parasite life cycle: bioluminescent Plasmodium in fundamental and applied research. *Front. Microbiol.* 6, 391
105. Costa, F.C. *et al.* (2018) Expanding the toolbox for Trypanosoma cruzi: a parasite line incorporating a bioluminescence-fluorescence dual reporter and streamlined CRISPR/Cas9 functionality for rapid *in vivo* localisation and phenotyping. *PLoS Negl. Trop. Dis.* 12, e0006388
106. Azevedo, M.F. *et al.* (2014) Plasmodium falciparum transfected with ultra bright NanoLuc luciferase offers high sensitivity detection for the screening of growth and cellular trafficking inhibitors. *PLoS One* 9, e112571–e112571
107. De Niz, M. *et al.* (2016) An ultrasensitive NanoLuc-based luminescence system for monitoring Plasmodium berghei throughout its life cycle. *Malar. J.* 15, 232
108. Hall, M.P. *et al.* (2012) Engineered luciferase reporter from a deep sea shrimp utilizing a novel imidazopyrazinone substrate. *ACS Chem. Biol.* 7, 1848–1857
109. Chu, J. *et al.* (2016) A bright cyan-excitable orange fluorescent protein facilitates dual-emission microscopy and enhances bioluminescence imaging *in vivo*. *Nat. Biotechnol.* 34, 760–767
110. Yeh, H.-W. *et al.* (2017) Red-shifted luciferase–luciferin pairs for enhanced bioluminescence imaging. *Nat. Methods* 14, 971–974
111. Kuchimaru, T. *et al.* (2016) A luciferin analogue generating near-infrared bioluminescence achieves highly sensitive deep-tissue imaging. *Nat. Commun.* 7, 11856
112. Iwano, S. *et al.* (2018) Single-cell bioluminescence imaging of deep tissue in freely moving animals. *Science* 359, 935–939
113. De Niz, M. *et al.* (2015) *In vivo* and *in vitro* characterization of a Plasmodium liver stage-specific promoter. *PLoS One* 10, e0123473
114. Cevenini, L. *et al.* (2014) Multicolor bioluminescence boosts malaria research: quantitative dual-color assay and single-cell imaging in Plasmodium falciparum parasites. *Anal. Chem.* 86, 8814–8821
115. Komatsu, N. *et al.* (2018) A platform of BRET–FRET hybrid biosensors for optogenetics, chemical screening, and in vivo imaging. *Sci. Rep.* 8, 8984
116. Niederhauser, J.J. *et al.* (2005) Combined ultrasound and optoacoustic system for real-time high-contrast vascular imaging *in vivo*. *IEEE Trans. Med. Imaging* 24, 436–440
117. Held, K.G. *et al.* (2016) Multiple irradiation sensing of the optical effective attenuation coefficient for spectral correction in handheld OA imaging. *Photoacoustics* 4, 70–80
118. Oraevsky, A.A. *et al.* (1994) Laser-based optoacoustic imaging in biological tissues. *Proc. SPIE* 2134, 122
119. Kruger, R.A. *et al.* (1995) Photoacoustic ultrasound (PAUS)-reconstruction tomography. *Med. Phys.* 10, 1605–1609
120. Weber, J. *et al.* (2016) Contrast agents for molecular photoacoustic imaging. *Nat. Methods* 13, 639
121. Beard, P. (2011) Biomedical photoacoustic imaging. *Interface Focus* 1, 602–631
122. Schwarz, M. *et al.* (2015) Implications of ultrasound frequency in optoacoustic mesoscopy of the skin. *IEEE Trans. Med. Imaging* 34, 672–677
123. Laufer, J. *et al.* (2009) Three-dimensional noninvasive imaging of the vasculature in the mouse brain using a high resolution photoacoustic scanner. *Appl. Opt.* 48, D299–D306
124. Yao, J. and Wang, L.V. (2014) Sensitivity of photoacoustic microscopy. *Photoacoustics* 2, 87–101
125. Hu, S. *et al.* (2011) Second-generation optical-resolution photoacoustic microscopy with improved sensitivity and speed. *Opt. Lett.* 36, 1134–1136
126. Wang, X. *et al.* (2006) Noninvasive imaging of hemoglobin concentration and oxygenation in the rat brain using high-resolution photoacoustic tomography. *J. Biomed. Opt.* 11, 24015
127. Razansky, D. *et al.* (2011) Volumetric real-time multispectral optoacoustic tomography of biomarkers. *Nat. Protoc.* 6, 1121–1129
128. Buehler, A. *et al.* (2010) Video rate optoacoustic tomography of mouse kidney perfusion. *Opt. Lett.* 35, 2475–2477
129. Taruttis, A. *et al.* (2010) Real-time imaging of cardiovascular dynamics and circulating gold nanorods with multispectral optoacoustic tomography. *Opt. Express* 18, 19592

130. Mercep, E. *et al.* (2015) Whole-body live mouse imaging by hybrid reflection-mode ultrasound and optoacoustic tomography. *Opt. Lett.* 40, 4643–4646
131. Bruce, M. *et al.* (2017) Limitations and artifacts in shear-wave elastography of the liver. *Biomed. Eng. Lett.* 7, 81–89
132. Chong, W.K. *et al.* (2018) Imaging with ultrasound contrast agents: current status and future. *Abdom. Radiol.* 43, 762–772
133. Errico, C. *et al.* (2015) Ultrafast ultrasound localization microscopy for deep super-resolution vascular imaging. *Nature* 527, 499
134. Kogan, P. *et al.* (2010) Microbubbles in imaging: applications beyond ultrasound. *Bubble Sci. Eng. Technol.* 2, 3–8
135. Grover, V.P.B. *et al.* (2015) Magnetic resonance imaging: principles and techniques: lessons for clinicians. *J. Clin. Exp. Hepatol.* 5, 246–255
136. Parlog, A. *et al.* (2014) Chronic murine toxoplasmosis is defined by subtle changes in neuronal connectivity. *Dis. Model. Mech.* 7, 459–469
137. Rodgers, J. *et al.* (2011) Magnetic resonance imaging to assess blood–brain barrier damage in murine trypanosomiasis. *Am. J. Trop. Med. Hyg.* 84, 344–350
138. Hoffmann, A. *et al.* (2017) *In vivo* tracking of edema development and microvascular pathology in a model of experimental cerebral malaria using magnetic resonance imaging. *J. Vis. Exp.* http://dx.doi.org/10.3791/55334
139. Tseng, C.-L. *et al.* (2010) Gadolinium hexanedione nanoparticles for stem cell labeling and tracking via magnetic resonance imaging. *Biomaterials* 31, 5427–5435
140. Ghaghada, K.B. *et al.* (2009) New dual mode gadolinium nanoparticle contrast agent for magnetic resonance imaging. *PLoS One* 4, e7628
141. Wessig, C. (2011) Detection of blood–nerve barrier permeability by magnetic resonance imaging. *Blood-Brain Other Neural Barriers Rev. Protoc.* 686, 267–271
142. Zheng, J. *et al.* (2009) MRI-based biomechanical imaging: initial study on early plaque progression and vessel remodeling. *Magn. Reson. Imaging* 27, 1309–1318
143. Aoki, I. *et al.* (2006) Cell labeling for magnetic resonance imaging with the T1 agent manganese chloride. *NMR Biomed.* 19, 50–59
144. Gilad, A.A. *et al.* (2008) MR tracking of transplanted cells with 'positive contrast' using manganese oxide nanoparticles. *Magn. Reson. Med.* 60, 1–7
145. Schmidt, R. *et al.* (2014) Highly shifted proton MR imaging: cell tracking by using direct detection of paramagnetic compounds. *Radiology* 272, 785–795
146. Germuska, M. and Bulte, D.P. (2014) MRI measurement of oxygen extraction fraction, mean vessel size and cerebral blood volume using serial hyperoxia and hypercapnia. *Neuroimage* 92, 132–142
147. Bulte, J.W.M. (2014) Science to practice: highly shifted proton MR imaging – a shift toward better cell tracking? *Radiology* 272, 615–617
148. Cromer Berman, S.M. *et al.* (2011) Tracking stem cells using magnetic nanoparticles: Wiley Interdiscip. *Rev. Nanomed. Nanobiotechnol.* 3, 343–355
149. Partlow, K.C. *et al.* (2007) ^{19}F magnetic resonance imaging for stem/progenitor cell tracking with multiple unique perfluorocarbon nanobeacons. *FASEB J.* 21, 1647–1654
150. Kadayakkara, D.K. *et al.* (2014) (19)F spin-lattice relaxation of perfluoropolyethers: dependence on temperature and magnetic field strength (7.0-14.1T). *J. Magn. Reson.* 242, 18–22
151. Srivastava, A.K. *et al.* (2015) Advances in using MRI probes and sensors for *in vivo* cell tracking as applied to regenerative medicine. *Dis. Model. Mech.* 8, 323–336
152. Pike, G.B. (2012) Quantitative functional MRI: concepts, issues and future challenges. *Neuroimage* 62, 1234–1240
153. Felder, J. *et al.* (2017) 9.4 T small animal MRI using clinical components for direct translational studies. *J. Transl. Med.* 15, 264
154. McDonald, C.R. *et al.* (2015) Experimental malaria in pregnancy induces neurocognitive injury in uninfected offspring via a C5a-C5a receptor dependent pathway. *PLoS Pathog.* 11, e1005140
155. van der Veen, D.R. *et al.* (2012) A 24-hour temporal profile of *in vivo* brain and heart pet imaging reveals a nocturnal peak in brain ^{18}F-fluorodeoxyglucose uptake. *PLoS One* 7, e31792–e31792
156. Baird, E. and Taylor, G. (2017) X-ray micro computed-tomography. *Curr. Biol.* 27, R289–R291
157. Chen, H. *et al.* (2013) Monitoring pH-triggered drug release from radioluminescent nanocapsules with X-ray excited optical luminescence. *ACS Nano* 7, 1178–1187
158. Rahmim, A. and Zaidi, H. (2008) PET versus SPECT: strengths, limitations and challenges. *Nucl. Med. Commun.* 29, 193–207